

Electrochemical Performance of Fe-Al intermetallic alloys with addition of Li, Ni and Ce in NaVO₃ at 700°C

A. Luna-Ramirez¹, J. Porcayo-Calderon^{2,*}, G. Salinas-Solano², C. D. Arrieta-Gonzalez³,
V.M. Salinas-Bravo¹ and L. Martinez⁴

¹Instituto de Investigaciones Eléctricas, 62490-Cuernavaca, Mor., México, Calle Reforma 113, Col. Palmira, 62490, Cuernavaca, Morelos, México.

²Universidad Autonoma del Estado de Morelos, CIICAp, Av. Universidad 1001, 62209-Cuernavaca, Morelos, Mexico

³Instituto Tecnológico de Zacatepec, Calzada Tecnológico 27, C.P. 62780, Zacatepec, Morelos, Mexico.

⁴Universidad Nacional Autónoma de México, Instituto de Ciencias Físicas, Av. Universidad s/n, Cuernavaca, Morelos, Mexico

*E-mail: jporcayoc@gmail.com

Received: 29 January 2013 / Accepted: 2 March 2013 / Published: 1 April 2013

Potentiodynamic polarization curves and polarization resistance measurements were used to study the hot corrosion behavior of two intermetallic compounds, i.e., FeAl and Fe₃Al with minor additions of Ni, Ce and Li exposed in a NaVO₃ salt at 700 °C. The results showed that the intermetallic alloys with single additions or co-doped disclosed better corrosion resistance than the FeAl based alloys. On the whole, the FeAl-Li intermetallic alloy had the greater resistance to hot corrosion. Since the FeAl and Fe₃Al intermetallic alloys without elements addition showed the greatest corrosion rate, the influence of the alloying elements on the corrosion behavior was of paramount importance.

Keywords: molten salt, intermetallic alloys, polarization curves, polarization resistance.

1. INTRODUCTION

Iron aluminides (Fe-Al) are intermetallic compounds that possess a number of advantages including low materials cost, low content of strategic elements (Ni and Cr), relatively low densities (Fe₃Al: 6.5 gcm⁻³, FeAl: 5.6 gcm⁻³) in comparison with the conventional Fe and Ni based alloys, corrosion resistance (in particular sulfidation) and oxidation resistance at high temperatures.

The oxidation resistance of these materials is due to the formation of an α -Al₂O₃ protective layer which plays an important role as a diffusion barrier. On the other hand, the addition of small amounts of elements such as Ce, Hf, La, Y, Zr, etc., can significantly improve the oxidation resistance of iron aluminides [1-3]. Rapp and Zhang [4] have shown that the Al₂O₃ is readily dissolved by molten salt such as alkali sulfates, and the general expectation suggest that iron aluminides, as with all Al₂O₃ forming alloys, will not be particularly resistant to molten salt related hot corrosion. Several authors have observed that such salts significantly increase the corrosion of Fe-Al alloys in SO₂ containing environments [5-7].

Fe₃Al based aluminides would be expected to have an excellent resistance to nitrate salt at lower temperatures (<600°C), or in nitrate salts that do not contain Na₂O₂. Preliminary results from exposure of FeAl to molten NaCl-Na₂CO₃ at 900°C indicated that its corrosion resistance is significantly better than that of Inconel 600 [8]. Recently, Salinas et al. [9] studied the effect of minor alloying elements (Ag, Cu, Li and Ni) on the corrosion behavior of Fe40Al in NaCl-KCl molten salts at 670°C by weight loss and potentiodynamic polarization, this study indicated that the addition of Li decreased the corrosion rate of unalloyed Fe40Al-base alloy, whereas the addition of Ag, Ni, or Cu increased it. Thus, the aim of this work was to assess the corrosion behavior using electrochemical techniques of two iron aluminides with and without addition of Ni, Ce and Li when exposed to sodium metavanadate (NaVO₃) at 700°C.

2. EXPERIMENTAL PROCEDURE

The intermetallic alloys used in this work were FeAl and Fe₃Al with additions of Li, Ce or Ni (1 at. %). The intermetallic alloys were produced by conventional casting. The alloying elements, either individual or combined, were added in 1 at.%. The mechanical properties and the microstructure of the intermetallic alloys used are described elsewhere [10].

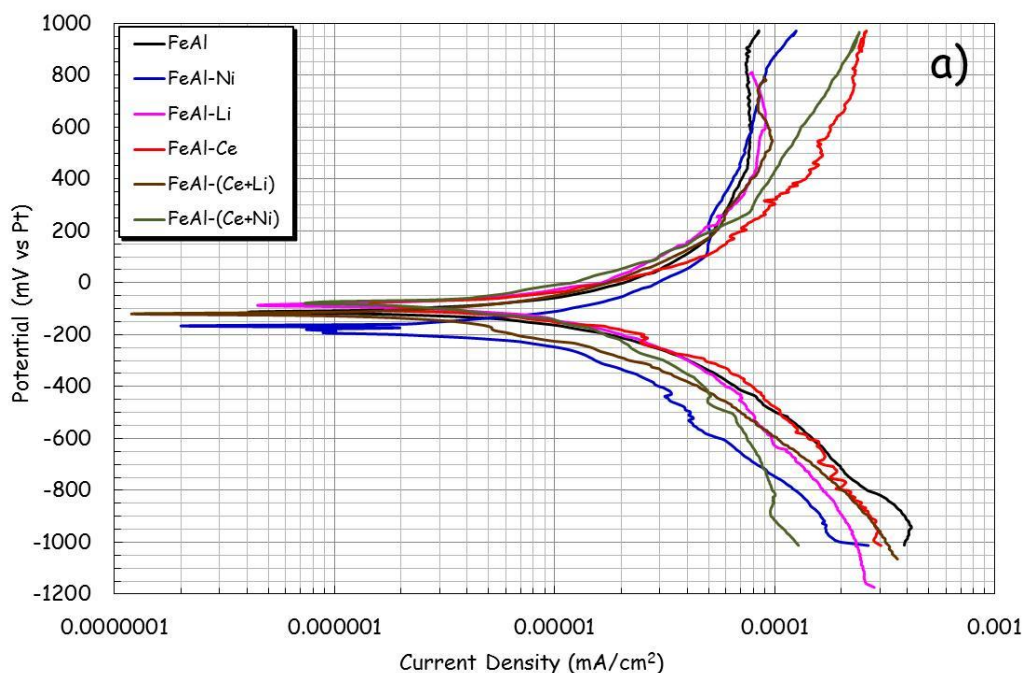
Electrochemical techniques, i.e. potentiodynamic polarization curves and linear polarization resistance (LPR) measurements, were applied. Details of the experimental set-up for the electrochemical cell used in this study are given elsewhere [11]. The amount of molten salt used was 500 mg/cm² under static air. The electrical contact in the working electrode was made by welding an 80Ni20Cr wire to the specimen. An automated potentiostat was used for all the electrochemical measurements. The working salt was NaVO₃ (analytical grade). The specimens (7x6x3 mm) were grinded with emery paper until 1200 grade, then washed with distilled water and degreased with acetone.

The potentiodynamic polarization tests were performed at ± 1000 mV respect to the rest corrosion potential (E_{corr}), and the scan rate was 1 mV/s, in agreement with ASTM G 59-91 standard [12]. Corrosion current density values, I_{corr} , were calculated by the Tafel extrapolation method. In the LPR measurements the working electrode was polarized at ± 10 mV at 1 mV/s respect to E_{corr} , and the data were taken every 30 min for 5 days. The testing temperature was 700°C. After the corrosion tests the specimens were analyzed in cross section by scanning electron microscope linked with a chemical analyzer (EDX) system used to obtain X-ray distribution maps.

3. RESULTS AND DISCUSSION

Figures 1 a) and 1 b) shows the effect of the minor alloying elements on the polarization curves for the FeAl and Fe₃Al base alloys at 700°C, respectively. Figure 1a shows that there are not significant differences in the anodic currents among the various intermetallic alloys. The FeAl, FeAl-Ni, FeAl-Li and FeAl-(Ce+Li) intermetallic alloys show current densities very similar between them. The current density increases slightly for the FeAl-(Ce+Ni) and FeAl-Ce alloys. After the linear portion of the anodic curve, all the intermetallics show certain instability, being the most unstable the FeAl-Ce alloy, which also disclosed the highest current density. These instabilities are probably originated by the detachment of corrosion products formed on the surface of the intermetallic alloys [13]. The FeAl alloy shows an attempt of passivation at potentials around 437 mV, which indicated a null increase in current density as the potential increases. The addition of Ni shifted the value of E_{corr} in directions slightly more active, although this alloy also shows a slight attempt of passivation between 125 and 250 mV. The FeAl-(Ce+Ni) and FeAl-Li alloys showed a slightly E_{corr} nobler than the FeAl base intermetallic. The addition of alloying elements did not influence on the formation of a passive region.

Figure 1b show that the current density of Fe₃Al intermetallic alloys decreases in the following order: Fe₃Al-(Ce+Ni), Fe₃Al-(Ce+Li), Fe₃Al, Fe₃Al-Li and Fe₃Al-Ni. The Fe₃Al-Ni alloy shows a passive region from 125 mV, and then exhibited a transpassive region around 625 mV where a current increase accompanied of oxide dissolution is observed. The Fe₃Al-Li alloy exhibits a passive region between 275 and 750 mV. The intermetallic alloys also show, after the linear portion slight instabilities, the most unstable being the Fe₃Al alloy. These instabilities are probably due to oxide detachment formed on the surface of the intermetallic alloys. The addition of Ni and Li have a major influence in the formation of a passive region.



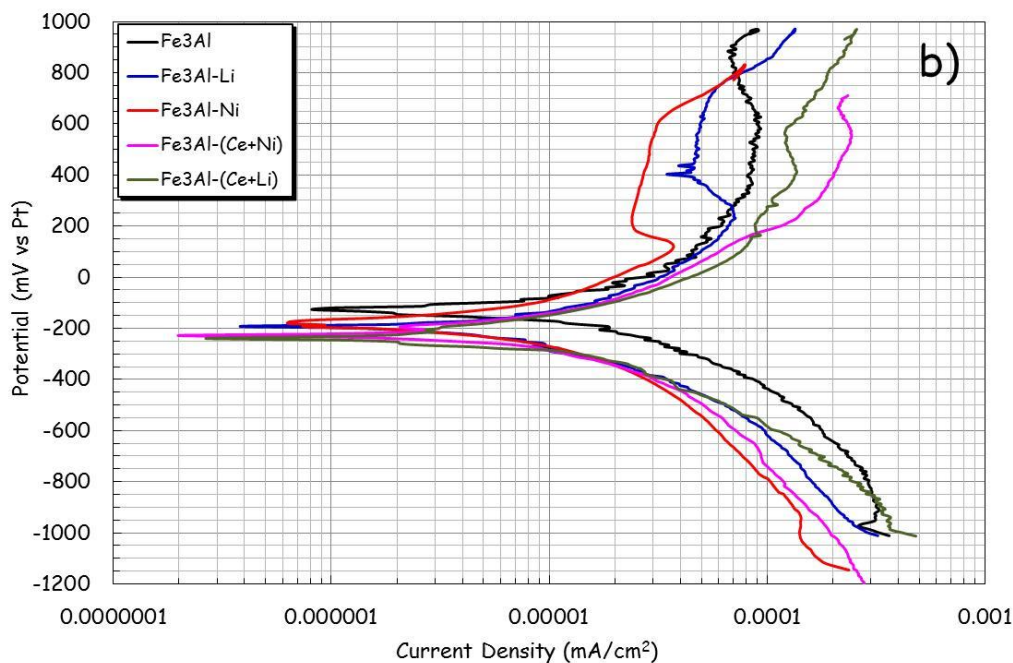


Figure 1. Polarization curves of a) FeAl and b) Fe₃Al intermetallic alloys in NaVO₃ at 700°C.

From the polarization curves, the anodic (b_a) and cathodic (b_c) slopes were obtained and these values were used to calculate the corrosion rates in terms of the current density (I_{corr}) of each intermetallic alloy. Table 1 gives a summary of the different electrochemical parameters obtained from the polarization curves.

Table 1. Electrochemical parameters obtained from polarization curves.

Intermetallic compound	b_c (mV/dec)	b_a (mV/dec)	E_{corr} (mV)
FeAl	-137.45	112.5	-112
FeAl-(Ce+Li)	-166.66	142.85	-118
FeAl-Ni	-140.0	80.0	-171
FeAl-Li	-128.20	112.36	-88
FeAl-Ce	-267.85	214.25	-72
FeAl-(Ce+Ni)	-200.0	185.7	-77
Fe ₃ Al	-212.5	175.0	-127
Fe ₃ Al-(Ce+Li)	-200.0	187.5	-240
Fe ₃ Al-Li	-163.93	158.73	-190
Fe ₃ Al-(Ce+Ni)	-189.87	181.81	-228
Fe ₃ Al-Ni	-160.0	100.0	-189

Figures 2 a) and 2 b) show the effect of the minor alloying elements on the I_{corr} curves obtained from the LPR tests for the FeAl and Fe₃Al base alloys at 700°C, respectively.

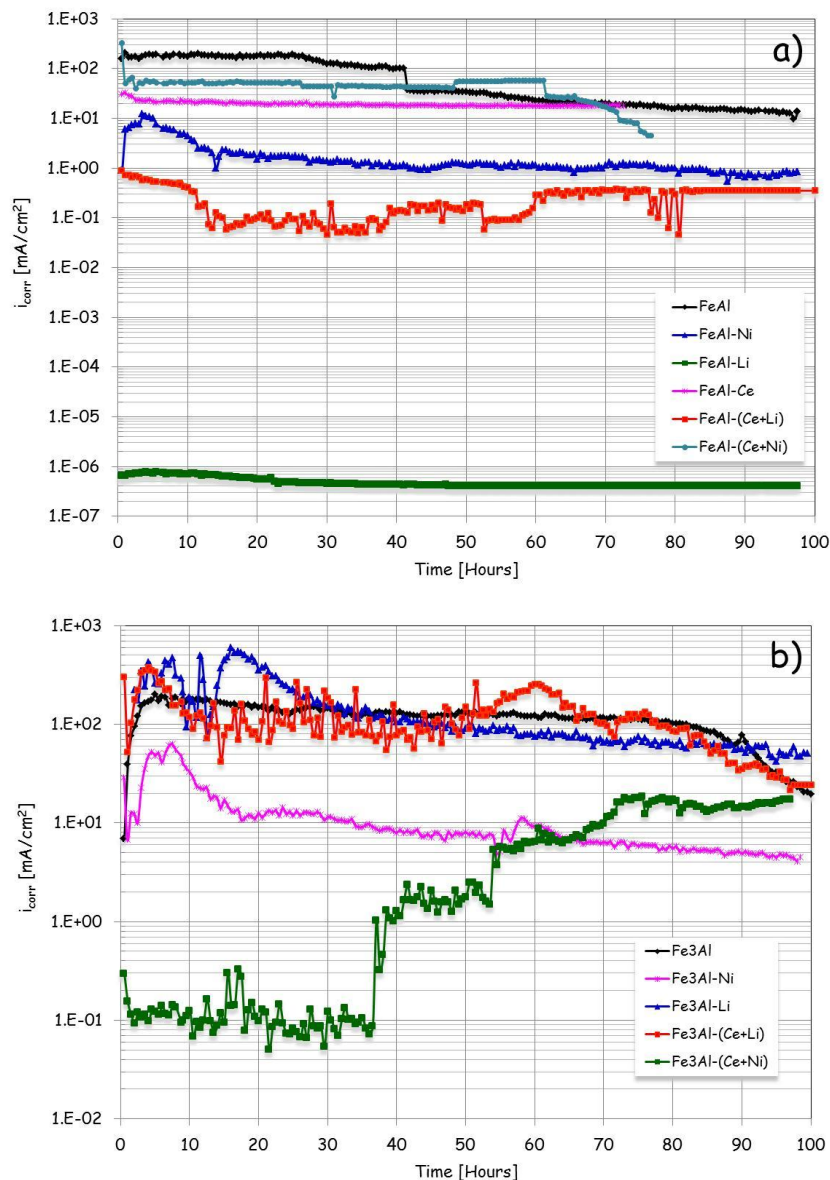


Figure 2. Change in I_{corr} with time for a) FeAl and b) Fe₃Al alloys in NaVO₃ at 700°C.

Figure 2a shows that almost all intermetallic alloys exhibited a decrease in the current density of corrosion with time, with I_{corr} values almost constant during the course of the tests, except the FeAl-(Ce+Li) alloy, which show very fluctuating values of I_{corr} . The FeAl-Li alloy exhibited the higher corrosion resistance, being the least resistant the FeAl and FeAl-(Ce+Ni) alloys, although the latter showed a decrease of the corrosion rate after approximately 40 hours of test; at the end of the test these two intermetallic alloys disclosed very narrow I_{corr} values.

The Fe₃Al-(Ce+Ni) (Figure 2b) alloy showed during the first 40 hours of test very fluctuating I_{corr} values. After 40 hours, the current density increases and finally it reaches I_{corr} values almost constant. This behavior is probably due to cracking or partial or total detachment of the oxide scale formed, allowing the entry of the salt towards the metal surface, and increasing the corrosion rate. This indicates that the oxide is unable to reform fast, since the degradation rate was higher than the oxide

scale formation rate. At the beginning of the test, I_{corr} values are very high in the Fe₃Al-Ni and Fe₃Al-(Ce+Li) intermetallic alloys (Figure 2b). The latter alloy show very variable values of I_{corr} during the first 55 hours of test. After this time these values reach certain stability with a decrease in the corrosion rate. The Fe₃Al-Ni alloy shows higher I_{corr} value after 6 hours of initiation of the test, and later I_{corr} exhibit a gradual decrease until the end of the test. The Fe₃Al alloy initiates with a low I_{corr} value, but this value increases during the first hours of the test, and later the corrosion rate diminishes showing a behavior very similar to the Fe₃Al-(Ce+Li) and Fe₃Al-Li alloys. The I_{corr} trends registered in all the intermetallic alloys do not clearly indicate which of the intermetallic alloys showed highest corrosion resistance. Nevertheless, bearing in mind the I_{corr} values to the end of every test, it is possible to say that the Fe₃Al-Ni alloy showed the best corrosion resistance and the Fe₃Al-Li alloy disclosed the highest corrosion rate.

A cross section of the FeAl, FeAl-Ce and FeAl-Li alloys corroded in NaVO₃ at 700°C and X-ray mapping for Al, Fe and V are presented in Figures 3-5. For the FeAl intermetallic (Figure 3) the presence of Al and Fe forming layered scales was detected, probably as Al₂O₃ and Fe₂O₃. The vanadium element was also detected and seems to be related to the Al- and Fe-layers, indicating that the oxides formed have been dissolved by the salt. The FeAl-Ce intermetallic (Figure 4) shows the presence of an Al-rich layer, probably Al₂O₃, adhering to the alloy. After this layer, a V-rich layer is found and seems to be related to the first one, this indicates that the salt penetrated and dissolved the oxide scale formed on the alloy and corroded the metal surface exposed to the salt. In the FeAl-Li intermetallic (Figure 5) the presence of Al was detected, but not in layers. Instead, it was dispersed in the vanadium-containing salt. Sodium was not detected in any of the intermetallic alloys, indicating, perhaps, that this element was evaporated [14].

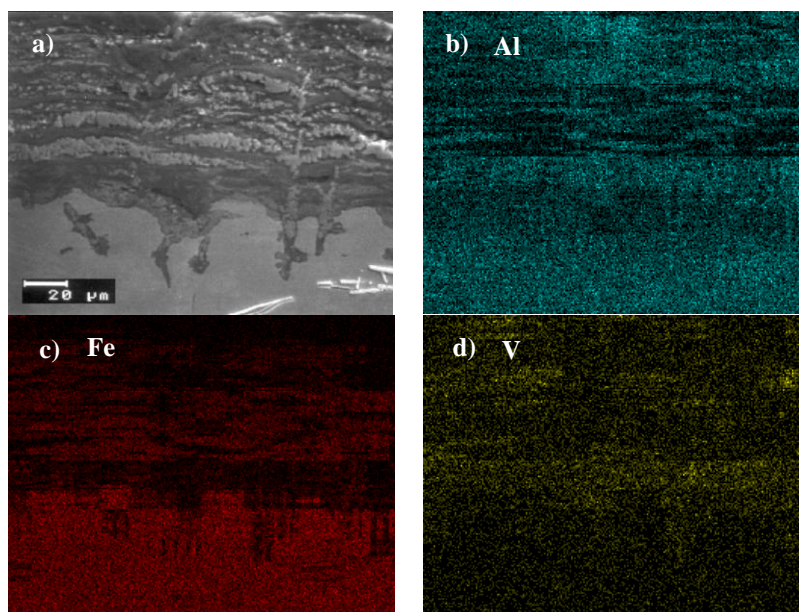


Figure 3. SEM micrograph in cross section of FeAl corroded in NaVO₃ at 700°C and X-ray maps for b) Al, c) Fe and d) V.

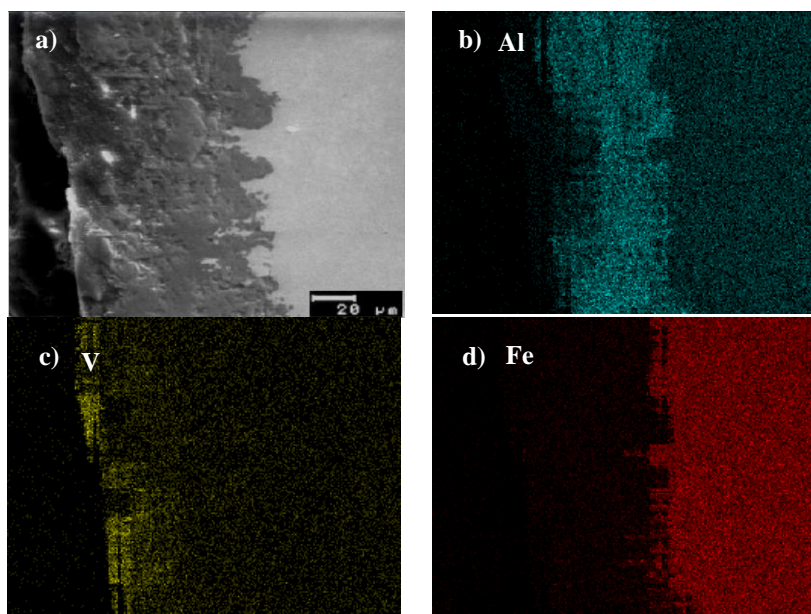


Figure 4. SEM micrograph in cross section of FeAl-Ce corroded in NaVO_3 at 700°C and X-ray maps for b) Al, c) V and d) Fe.

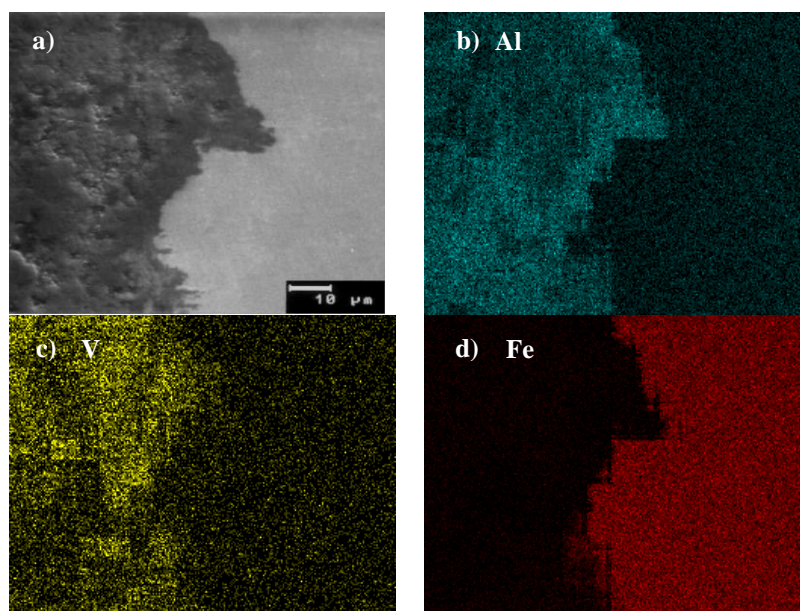


Figure 5. SEM micrograph in cross section of FeAl-Li corroded in NaVO_3 at 700°C and X-ray maps for b) Al, c) V and d) Fe.

Cross sectional micrographs of the Fe_3Al , $\text{Fe}_3\text{Al}-(\text{Ce}+\text{Ni})$, $\text{Fe}_3\text{Al}-\text{Ni}$ and $\text{Fe}_3\text{Al}-(\text{Ce}+\text{Li})$ alloys corroded in NaVO_3 at 700°C and X-ray mapping for Al, Fe and V are shown in Figures 6-10. The X-ray mapping for Al obtained for the Fe_3Al alloy (Figure 6) makes evident the presence of two Al-layers, the first layer is adhered to the alloy probably in the form of Al_2O_3 , and the second layer is far from the metal/oxide interface showing evidence of dissolution of the oxide scale formed due to the molten salts. The vanadium associated with the internal Al-layer has penetrated up to the alloy,

indicating that the possible Al_2O_3 formed has been dissolved by the vanadium salts and has corroded the substrate. This might explain the greater rate corrosion showed by this intermetallic alloy. The X-ray maps obtained from the $\text{Fe}_3\text{Al}-(\text{Ce}+\text{Ni})$ (Figure 7) alloy indicate the presence of an Al-rich layer, in the form of Al_2O_3 . It was also detected a Fe-rich layer, probably Fe_2O_3 , with both layers localized far from of the interface. Underneath these layers a V-rich layer was detected. This suggests that the oxide formed has been penetrated and dissolved by the molten salt. The elements distribution in the $\text{Fe}_3\text{Al}-\text{Ni}$ alloy (Figure 8) shows the presence of a thin Fe-layer close to the base metal. After this one a thick corrosion products layer was observed, and the presence of this thick layer could have limited the access of molten salts fresh and therefore a decline in its corrosion rate was detected. The X-ray maps carried out on the corrosion products of the $\text{Fe}_3\text{Al}-(\text{Ce}+\text{Li})$ alloy (Figure 9) indicates the presence of two internal Al- and Fe- layer adhered to the metal base, probably in the form of Al_2O_3 y Fe_2O_3 , respectively.

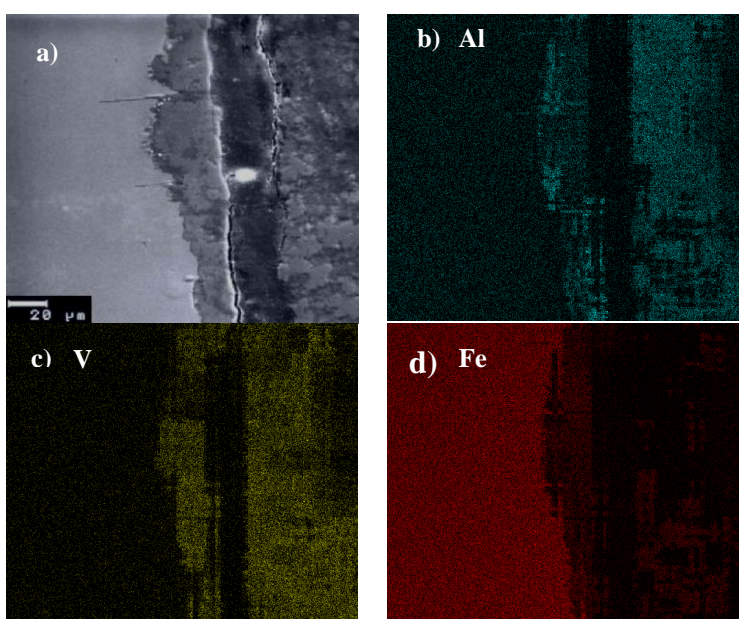
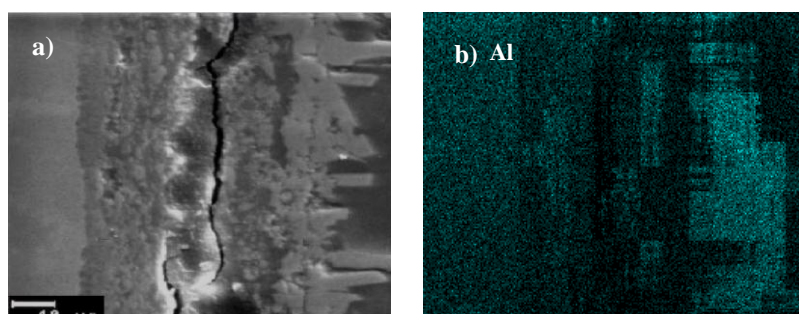


Figure 6. SEM micrograph in cross section of Fe_3Al corroded in NaVO_3 at 700°C and X-ray maps for b) Al, c) V and d) Fe.



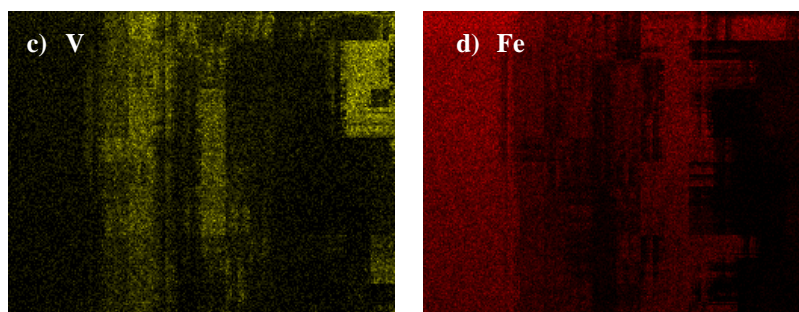


Figure 7. SEM micrograph in cross section of $\text{Fe}_3\text{Al}-(\text{Ce}+\text{Ni})$ corroded in NaVO_3 at 700°C and X-ray maps for b) Al, c) V and d) Fe.

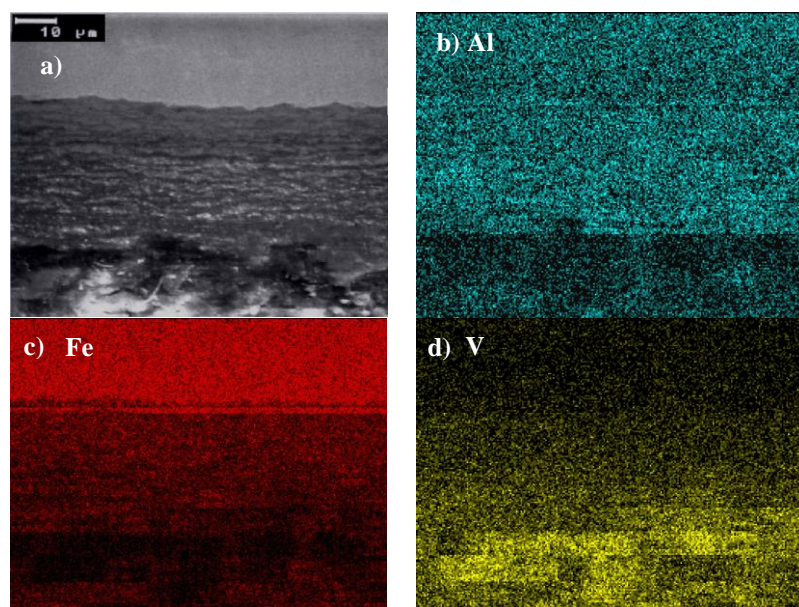
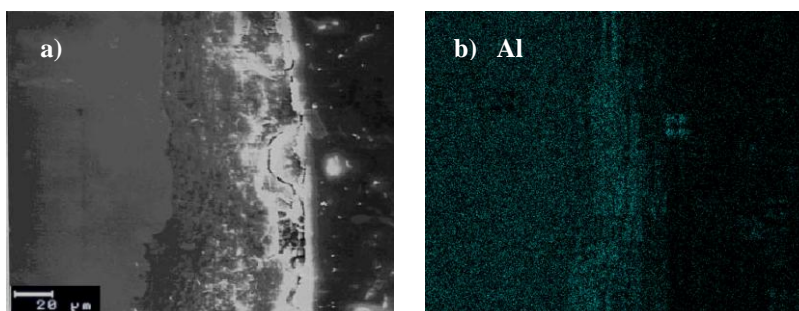


Figure 8. SEM micrograph of $\text{Fe}_3\text{Al-Ni}$ corroded in NaVO_3 at 700°C and X-ray maps for b) Al, c) Fe and d) V.

Also, two V-layers were detected, a first layer poor in vanadium but associated to the Al- and Fe- layers. This V layer indicates that the oxide formed has been attacked by the molten salts, the second layer (external) contains higher V content but localized on the oxide scale formed. For the $\text{Fe}_3\text{Al-Li}$ intermetallic (Figure 10) the presence of Al and Fe was detected, but not in layers; instead, they were dispersed in the vanadium-containing salt. Sodium was also not detected in any of the intermetallic alloys.



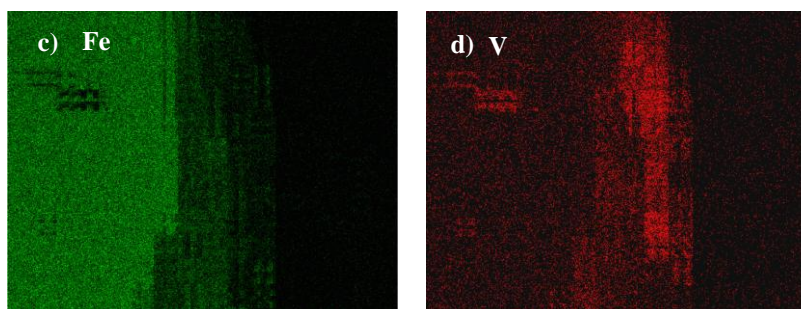


Figure 9. SEM micrograph cross section of $\text{Fe}_3\text{Al}-(\text{Ce}+\text{Li})$ corroded in NaVO_3 at 700°C and X-ray maps for b) Al, c) Fe and d) V.

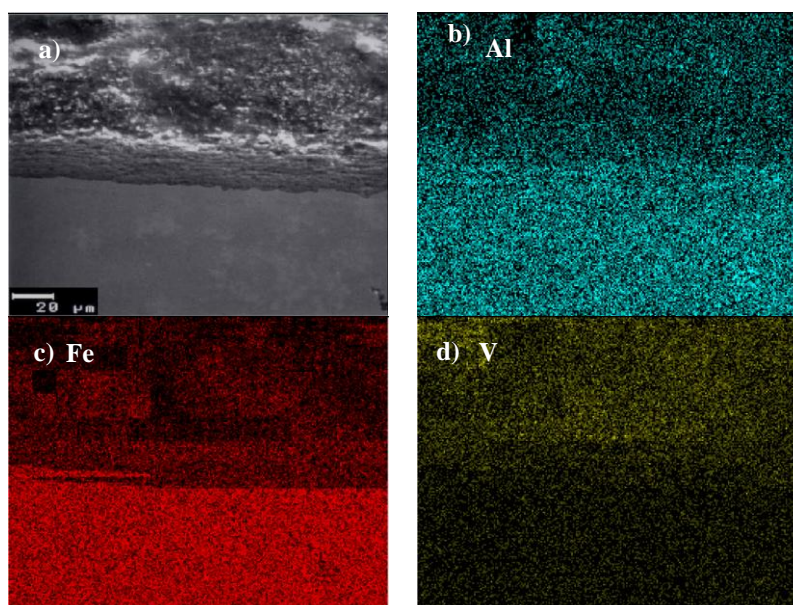
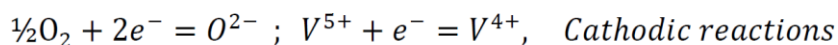
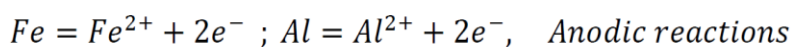


Figure 10. SEM micrograph in cross section of $\text{Fe}_3\text{Al-Li}$ corroded in NaVO_3 at 700°C and X-ray maps for b) Al, c) Fe and d) V.

Any electrochemical corrosion reaction consists at least of two electrochemical partial reactions, the anodic reaction of the dissolution of a metal M ($M = M^{n+} + ne^-$) and the cathodic partial reaction of the reduction of an oxidizing species Ox ($\text{Ox} + me^- = \text{Red}^{m-}$) [15]. For the case of Fe-Al based intermetallics, whose main alloying elements are Al and Fe, the anodic reactions of metal dissolution in the metal/salt interface and the cathodic reaction of the reduction in the salt/gas interface are:



The formation of metal ions (Fe^{2+} y Al^{2+}) and the detection of an oxide scale (metal ions react with the oxide ion to form the metal oxide) suggest that the hot corrosion mechanism is one of electrochemical nature [16]. The solubility of many oxides increases when increasing the acidity or basicity of the fused salt, then the solubility of the oxide is high in the metallic surface and decreases towards the exterior of the fused salt, in such a way that the oxides are dissolved in the salt/oxide interface and reprecipitate in the salt to a particular distance of the surface where the acidity or basicity is below of a certain critical value [17]. This agrees with the observations in the micrographs and the X-ray mapping corresponding to the corrosion products of the intermetallic compounds, since an oxide, very likely Al_2O_3 , has precipitated far from the metal surface and the element vanadium was detected on the surface of the base metal, which indicates that the oxide formed has been dissolved by the salt.

In practice, all the intermetallic alloys showed at the beginning of the experiment high I_{corr} values i.e. an increase in corrosion rate. As function of time, the corrosion rate diminished (except for the $\text{Fe}_3\text{Al}-(\text{Ce}+\text{Li})$ intermetallic). This is consistent with the growth of an oxide scale on the surface of the metal. Nevertheless, at the test temperature used in this work (700°C), the most probable situation is that the oxide formed is of the type $\gamma\text{-Al}_2\text{O}_3$ [18]. This oxide is considered to be non-protective, of poor adherence due to its high concentration of vacancies, non-uniform, with a porous microstructure and of fast growth [19-21]. Simultaneously, the protective scale is destroyed or eliminated by the fluxing action of the molten salt and consequently the surface metal is exposed to direct action of the aggressive environment as has been observed in the present work. Also, it has been reported that the presence of vanadium and its oxidized product generates compounds with aciculate morphology, which do not cover in appropriate way the metallic surface and contributes to reduce the protective character of the scale [22]. This features and the cracks observed in Figure 7, could help to explain the $\text{Fe}_3\text{Al}-(\text{Ce}+\text{Ni})$ intermetallic behavior showed during the test i.e., at the beginning of the test an oxide scale is formed causing a very low corrosion rate. Later, due to the dissolution of the oxide scale, the degradation rate of the substrate was greater being reflected as an increase in the corrosion rate values recorded.

A comparison of results from I_{corr} between both Fe-Al systems indicates that the FeAl alloys were more resistant to corrosion than the Fe_3Al intermetallic alloys. A possible explanation could be that the Fe_3Al has a tendency for scale spallation. This is likely due to the very large difference in thermal expansion coefficients of Al_2O_3 and Fe_3Al . This fact will facilitate the attack of the fused salt on the metal surface, producing an increase in corrosion rates. Further, the FeAl alloys have a higher content of Al and it has been demonstrated that alloys richer in Al are more resistant to the corrosion. The literature [23, 24] seems to indicate that the addition of alloying elements or reactive elements do not have influence on the corrosion resistance of the Fe-Al intermetallic alloys. Although other studies [25] have shown that the addition of alloying elements such as chromium and titanium decrease the corrosion rate of the base alloy FeAl40 base alloy.

In this research, some influence of the alloying elements is observed, although this was not very consistent; i.e., addition of Li and (Li+Ce) seems to improve the corrosion resistance in the FeAl intermetallic, Salinas et al. [9] found similar behavior of the Li (1 at. %) in FeAl40 based alloys in $\text{NaCl} + \text{KCl}$ molten salt at 670°C , but not in the case for the Fe_3Al base alloys (the FeAl-Li and FeAl-(Ce+Li) intermetallics showed values of I_{corr} lower than the $\text{Fe}_3\text{Al-Li}$ and $\text{Fe}_3\text{Al}-(\text{Ce}+\text{Li})$ alloys). The

addition of Ni produced values of I_{corr} very similar, that is; the FeAl-Ni and Fe₃Al-Ni alloys had very similar corrosion resistance. The addition of (Ce+Ni) in the FeAl and in the Fe₃Al intermetallic alloys also generated different behaviors. Finally, the FeAl and Fe₃Al intermetallic alloys showed the highest corrosion rate values, which implies that the addition of the alloying elements somehow influenced the alloys corrosion behavior. Oxidation studies [11] show that the FeAl-Li and FeAl-(Ce+Li) alloys showed a decrease in voids formation at the metal/oxide interface, increasing the scale adherence, and the oxide formed was dense and of fine grain size. This might explain why both intermetallic alloys showed the best corrosion resistance. These alloying elements did not have the same effect on the Fe₃Al alloys, and this inconsistency make difficult to establish with precision the effect of the alloying elements on the corrosion behavior, since both the Fe₃Al-Li and the Fe₃Al-(Ce+Li) showed higher corrosion rates than the FeAl-Li and FeAl-(Ce+Li) intermetallics.

4. CONCLUSIONS

The FeAl and Fe₃Al base alloys showed the highest corrosion rates, and the FeAl-Li and FeAl-(Ce+Li) intermetallics showed better corrosion resistance than the FeAl-Ce, FeAl-(Ce+Ni) and FeAl-Ni intermetallics. For the Fe₃Al system, the Fe₃Al-Ni alloy showed the best corrosion resistance, being the Fe₃Al-Li alloy the less corrosion resistant material, the addition of Ni and Li to Fe₃Al seems to have major influence in the formation of a passive region. It was observed a certain influence of the alloying elements on the corrosion rate, although this influence was not consistent to all the intermetallic alloys at the same experimental conditions. On the whole, the FeAl-Li intermetallic alloy has the greater resistance to hot corrosion, under the conditions of the present work.

References

1. M.P. Brady, B.A. Pint, P.F. Tortorelli, I.G. Wright and R.J. Hanrahan, in *Corrosion and Environmental Degradation*, M. Schutze (Ed), Wiley-VCH Verlag W., 2002.
2. S.C. Deevi, V. K. Sikka, *Intermetallic* 4 (1996) 357-375.
3. N.S. Stoloff, *Mater. Sci. and Eng., A* 258 (1998) 1-14.
4. R.A. Rapp and Zhang Y.S., *Molten Salt Forum* 5-6 (1998) 25-38.
5. W. H. Lee and R.Y. Lin in R.R. Judkins, D.N. Braski (Eds.) *Fourth Annual Conf. Fossil Energy Materials* (1990) 475-486.
6. W. Niu and Y. Guo, in *High Temperature Corrosion of Advanced Materials and Protective Coatings*. Satio Y., Onay B., Maruyama T., (Eds.) Elsevier Science (1992).
7. F. Gesmundo, Y. Niu, F. Viani and O. Tassa, *Journal de Physique IV, Colloque C9*. Supplement au Journal de Physique II, 3 (1993).
8. J. C. Newcomb, D. L. Grimmet and R. L. Gray, *Energy Tech. Eng. Center Report*, (1995) 022-ZR-004.
9. G. Salinas, J.G. Gonzalez-Rodriguez, J. Porcayo-Calderon, V.M. Salinas-Bravo and M.A. Espinosa-Medina, *International Journal of Corrosion*, vol. 2012, Article ID 185842, 7 pages, 2012. doi:10.1155/2012/185842.
10. M.M. Salazar, *Tesis Doctoral*, México, D. F., UNAM, 2001.
11. A. Luna-Ramírez, *Ph.D. Thesis*, CIMAV-México, 2006.

12. ASTM G 59-91, *Standard Practice for Conducting Potentiodynamic Polarization Resistance Measurement*.
13. L. Martínez, M. Amaya, J. Porcayo-Calderon and E. J. Lavernia, *Mat. Sci. Eng.*, A258 (1998) 306-312.
14. M.A. Espinosa-Medina, M. Casales M, A. Martínez-Villafane, J. Porcayo-Calderon, L. Martínez L., J. G. Gonzalez-Rodriguez, *Mat. Sci. and Eng. A* 300 (2001) 183-189.
15. A. Rahmel, *Mat. Sci. Eng.*, 87 (1987)345-352.
16. A. Rahmel, M. Schmidt and M. Schorr M., *Oxid. Met.*, 18 (1982)195-223.
17. R. A. Rapp, *Corrosion Science*, 44 (2002) 209-221.
18. H. J. Grabke, *Mat. Sci. Forum*, 251-254 (1997) 149-162.
19. P.F. Tortorelli and K. Natesan, *Mat. Sci. Eng.*, A-258 (1998) 115-125.
20. M. Sakiyama, P. Thomaszeweiz and G.R. Wallwork, *Oxid. Met.*, 13 (1979) 311.
21. B. A. Pint in: D.A. Shores, R.A. Rapp, P.Y. Hou (Eds.), *The Electrochemical Society*, (1997) 74.
22. H. Singh, D. Puri, S. Prakash and T. K. Ghosh, *Mat. Corr.*, 58 No. 11 (2007) 857-866.
23. W.U. Weitao and N. Y. Guo, *High-Temperature Corrosion of Advanced Materials and Protective Coatings*, Elsevier Science Publishers B. V (1992).
24. M. A. Espinosa, *Ph.D. Thesis*. CIMAV- México (2001).
25. R. Ademar, J. G. Gonzalez-Rodriguez, J. Uruchurtu, J. Porcayo-Calderon, V.M. Salinas-Bravo, G. Dominguez-Patiño and A. Bedolla-Jacuinde, *International Journal of Corrosion*, vol. 2012, Article ID 146486, 9 pages, 2012. doi:10.1155/2012/146486.